Hypoxia-inducible factor prolyl-4-hydroxylation in FOXD1 lineage cells is essential for normal kidney development

see commentary on page 1314

Hanako Kobayashi[1,2], Jiao Liu[3,4], Andres A. Urrutia[1], Mikhail Burmakin[5], Ken Ishii[1], Malini Rajan[1], Olena Davidoff[1,2], Zubaida Saifudeen[3,4] and Volker H. Haase[1,2,6]

[1]Department of Medicine, Vanderbilt University School of Medicine, Nashville, Tennessee, USA; [2]Medical and Research Services, Department of Veterans Affairs Hospital, Tennessee Valley Healthcare System, Nashville, Tennessee, USA; [3]Section of Pediatric Nephrology, Department of Pediatrics, Tulane University Health Sciences Center, New Orleans, Louisiana, USA; [4]The Hypertension and Renal Centers of Excellence, Tulane University Health Sciences Center, New Orleans, Louisiana, USA; [5]Division of Vascular Biology, Department of Medical Biochemistry and Biophysics, Karolinska Institute, Stockholm, Sweden; and [6]Department of Cancer Biology and Department of Molecular Physiology and Biophysics, Vanderbilt University School of Medicine, Nashville, Tennessee, USA

Hypoxia in the embryo is a frequent cause of intra-uterine growth retardation, low birth weight, and multiple organ defects. In the kidney, this can lead to low nephron endowment, predisposing to chronic kidney disease and arterial hypertension. A key component in cellular adaptation to hypoxia is the hypoxia-inducible factor pathway, which is regulated by prolyl-4-hydroxylase domain (PHD) dioxygenases PHD1, PHD2, and PHD3. In the adult kidney, PHD oxygen sensors are differentially expressed in a cell type–dependent manner and control the production of erythropoietin in interstitial cells. However, the role of interstitial cell PHDs in renal development has not been examined. Here we used a genetic approach in mice to interrogate PHD function in FOXD1-expressing stroma during nephrogenesis. We demonstrate that PHD2 and PHD3 are essential for normal kidney development as the combined inactivation of stromal PHD2 and PHD3 resulted in renal failure that was associated with reduced kidney size, decreased numbers of glomeruli, and abnormal postnatal nephron formation. In contrast, nephrogenesis was normal in animals with individual PHD inactivation. We furthermore demonstrate that the defect in nephron formation in PHD2/PHD3 double mutants required intact hypoxia-inducible factor-2 signaling and was dependent on the extent of stromal hypoxia-inducible factor activation. Thus, hypoxia-inducible factor prolyl-4-hydroxylation in renal interstitial cells is critical for normal nephron formation.

Kidney International (2017) **92,** 1370–1383; http://dx.doi.org/10.1016/j.kint.2017.06.015

KEYWORDS: chronic kidney disease; hypoxia; hypoxia-inducible factor; pericytes; prolyl-4-hydroxylase; renal development

Correspondence: *Volker H. Haase, Department of Medicine, Division of Nephrology & Hypertension, Vanderbilt University Medical Center, C-3119A MCN, 1161 21st Avenue So., Nashville, Tennessee 37232-2372, USA. E-mail: volker.haase@vanderbilt.edu*

Received 28 October 2016; revised 26 May 2017; accepted 8 June 2017; published online 1 September 2017

Hypoxia occurs not only under pathologic conditions but also physiologically during normal development and regulates stem cell behavior, cellular differentiation, proliferation, and migration, as well as the reciprocal interactions between different cell types on multiple levels, thus affecting the morphogenesis of the embryo and placenta. Therefore, molecular mechanisms that permit cells to adequately respond to discrepancies between oxygen demand and supply are critically important for normal embryonic development. A disruption of these responses may lead to developmental abnormalities in multiple organ systems and in worst case scenario to intraembryonic demise.[1]

A major and critical component of cellular hypoxia responses is the prolyl-4-hydroxylase domain (PHD)-hypoxia-inducible factor (HIF) axis, which enables cells to respond to changes in tissue oxygen levels in a rapid and controlled manner. HIF-1 and HIF-2 are pleiotropic basic helix-loop-helix transcription factors that consist of an oxygen-sensitive α-subunit and a constitutively expressed β-subunit, also known as the aryl hydrocarbon receptor nuclear translocator. HIF transcription factors regulate a multitude of hypoxia responses allowing cells to adapt to and survive low oxygen environments.[2] Under normoxic conditions, the oxygen-, iron-, and 2-oxoglutarate-dependent PHD proteins PHD1, PHD2, and PHD3, also known as egl nine homolog (EGLN)2, EGLN1, and EGLN3, respectively, function as oxygen sensors of HIF pathway. PHD enzymes initiate rapid proteasomal degradation of constitutively synthesized HIF-α subunits through the hydroxylation of specific proline residues.[3] A reduction in PHD catalytic activity, for example, under hypoxic conditions or owing to pharmacologic inhibition, results in HIF-α stabilization and activation of HIF transcriptional programs.[3]

Sustained discrepancies between oxygen demand and supply can result from maternal disease, uteroplacental insufficiency, or exposure to high altitude. This frequently leads to intrauterine growth retardation and low birth weight and increases the risk of developing diabetes, cardiopulmonary disease, stroke, arterial hypertension, or chronic kidney

disease in adults.[4–6] In the developing kidney, hypoxia reduces ureteric bud (UB) branching and nephron formation[7] and results in low nephron endowment, which by itself is associated with an increased risk of chronic kidney disease and/or arterial hypertension.[8,9]

Normal kidney development is driven by multiple reciprocal and cyclical interactions between UB and metanephric mesenchyme, which result in repeated UB branching and nephron formation.[10,11] However, little is known about the role of stromal cells in this process. The renal stroma is identified by the expression of the forkhead box D1 (FOXD1) transcription factor and surrounds the cap mesenchyme (CM). FOXD1-expressing stroma plays a critical role in renal capsule development, renal progenitor differentiation, and nephron formation; is important for normal vascular patterning; and ultimately gives rise to cortical and medullary interstitial fibroblast-like cells, pericytes, mesangial cells, and vascular smooth muscle cells.[12–17] Because hypoxia physiologically occurs during kidney development, both HIF-1α and HIF-2α have been detected in the developing kidney in a cell type–dependent manner.[18–20] However, despite clear evidence of HIF pathway activation, the functional roles of cell-specific HIF signaling during renal development are poorly understood, and information from genetic models is limited.

To examine the role of interstitial HIF oxygen sensing in renal development and homeostasis, we used the Cre-loxP system to target all 3 HIF-PHDs in conjunction with HIF-1α or HIF-2α in FOXD1-expressing stromal cells. We found that mice with individual *Phd1*, *Phd2,* or *Phd3* deletion or *Phd1-Phd2* and *Phd1-Phd3* double deletion were born with normal kidneys, whereas the combined inactivation of *Phd2* and *Phd3* resulted in abnormal kidney development, renal failure, and premature death. Kidney defects in *Phd2-Phd3* double-knockout mice became apparent after postnatal day (P) 7, correlated with the degree of interstitial HIF activation and were characterized by a HIF-2–dependent reduction in the number of mature nephrons and glomeruli as well as abnormal renal vasculature. Taken together, our data establish that the ability to regulate HIF prolyl-4-hydroxylation in FOXD1 stroma–derived cells is essential for normal nephron formation. Our data have implications for the therapeutic use of HIF prolyl-4-hydroxylase inhibitors, which are currently in phase 3 clinical development for renal anemia.[21]

RESULTS

Combined inactivation of *Phd2* and *Phd3* in FOXD1 stroma is associated with renal failure and juvenile lethality

Interstitial cells play an important role in the regulation of renal hypoxia responses. A classic example is the hypoxic induction of *erythropoietin* (EPO). To examine the role of individual PHDs in these responses, we utilized $Foxd1^{cre/+}$ transgenic mice. In this transgenic line, the *Cre* transgene, which consists of an enhanced green fluorescent protein–Cre-recombinase fusion protein, is under the transcriptional control of the *Foxd1* promoter (Figure 1a).[22,23] FOXD1-expressing cells surround the CM in the nephrogenic zone, give rise to all stromal components of the developing kidney and express *Phd1*, *Phd2,* and *Phd3* (Supplementary Figure S1).

Utilizing $Foxd1^{cre/+}$ transgenic mice, we developed mice with individual or combined inactivation of PHD1, PHD2, and PHD3. $Foxd1^{cre/+}$ $Phd1^{fl/fl}$, $Foxd1^{cre/+}$ $Phd2^{fl/fl}$, *and* $Foxd1^{cre/+}$ $Phd3^{fl/fl}$ mutant mice (hereon referred to as *Foxd1-Phd1*$^{-/-}$, *Foxd1-Phd2*$^{-/-}$, *and Foxd1-Phd3*$^{-/-}$ mutants, respectively) developed normally into adulthood, whereas $Foxd1^{cre/+}$ $Phd2^{fl/fl}$ $Phd3^{fl/fl}$ double-knockout mice (hereon referred to as *Foxd1-Phd2*$^{-/-}$*-Phd3*$^{-/-}$ mutants) were small and died prematurely (Figure 1b). Differences in whole-body weight between mutants and Cre^{-} littermate controls ($Foxd1^{+/+}$ $Phd2^{fl/fl}$ $Phd3^{fl/fl}$) became statistically significant by P14 (5.0 ± 0.4 g vs. 7.3 ± 0.5 g; n = 8 and 12, respectively; $P = 0.003$; Supplementary Table S1). Juvenile lethality in the mutant cohort was associated with renal failure and severe pathologic changes in the kidney (Figures 1c and d). Kidney weight in mutants was significantly reduced compared with that in controls (28.2 ± 2.1 mg vs. 47.9 ± 2.5 mg; n = 16 and 24, respectively; $P < 0.0001$; Supplementary Table S1), and renal defects in *Foxd1-Phd2*$^{-/-}$*-Phd3*$^{-/-}$ mutants at weaning age were characterized by tubular and vascular dilatations, tubular cyst formation, accumulation of α-smooth muscle actin (alpha actin-2 [ACTA2])–positive interstitial and glomerular cells, glomerular sclerosis, increase in collagen matrix and *collagen type 1 alpha 1* mRNA production, and increased *F4/80* mRNA levels (Figure 1e and f; Supplementary Figure S2). Because PHD inhibition results in normoxic HIF-α stabilization and HIF signaling activation, we assessed mRNA expression levels of HIF target gene *Epo*. Despite the presence of severe morphologic defects, *Epo* mRNA levels in the kidney were significantly increased in 2-week-old *Foxd1-Phd2*$^{-/-}$*-Phd3*$^{-/-}$ mice, indicating that the combined deletion of *Phd2* and *Phd3* resulted in the robust activation of the HIF system in FOXD1 stroma–derived interstitial cells (an approximate 80-fold increase; n = 9 and 10, respectively; $P <$ 0.0001; Figure 1e). Increased *Epo* was accompanied by a small but significant increase in hematocrit levels (38.8% ± 1.1% in mutants and 35.5% ± 0.8% in controls; n = 14 and 14, respectively; $P < 0.05$).

Because HIF is known to promote angiogenesis,[24,25] we examined the renal vasculature in *Foxd1-Phd2*$^{-/-}$*-Phd3*$^{-/-}$ kidneys. For this, we used real-time polymerase chain reaction (PCR) in conjunction with immunohistochemistry to characterize the tissue expression patterns of ACTA2 and endothelial cell marker cluster of differentiation (CD)31. On P14, we observed significant increases in microvessel density, which correlated with elevated *Cd31* mRNA expression levels in whole-kidney homogenates (approximately 1.4-fold increase; Figure 1f). Furthermore, small- and medium-sized arterial vessels in *Foxd1-Phd2*$^{-/-}$*-Phd3*$^{-/-}$ kidneys were dilated and characterized by relatively thin vessel walls (Figure 1d). Vascular changes in *Foxd1-Phd2*$^{-/-}$*-Phd3*$^{-/-}$ kidneys were associated with increased transcription of *vascular endothelial growth factor* in the renal interstitium, as

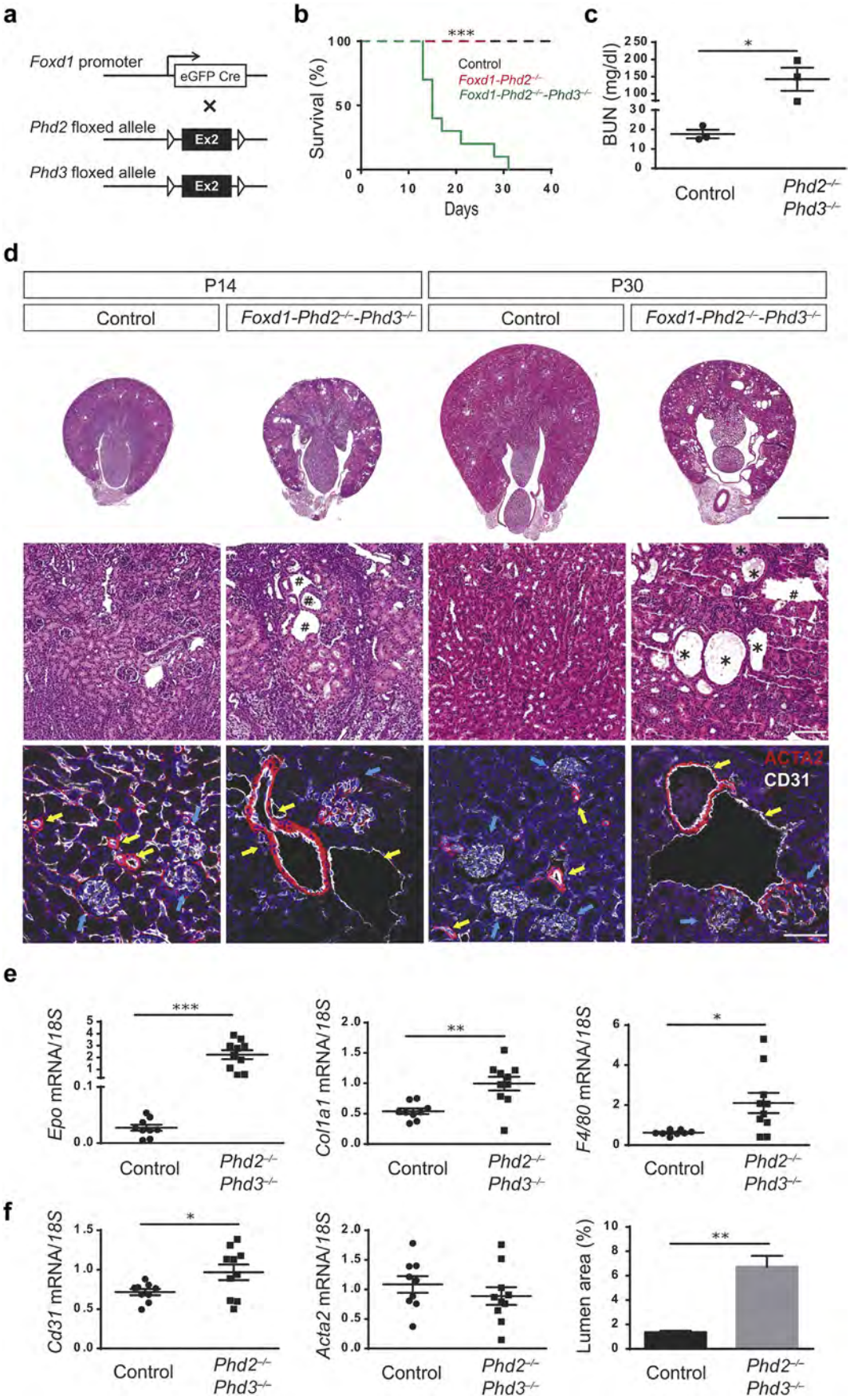
a
Foxd1 promoter
eGFP Cre
×
Phd2 floxed allele
Ex2
Phd3 floxed allele
Ex2
b
***
Control
Foxd1-Phd2−/−
Foxd1-Phd2−/−-Phd3−/−
Survival (%)
Days
c
*
BUN (mg/dl)
Control
Phd2−/−
Phd3−/−
d
P14
P30
Control
Foxd1-Phd2−/−-Phd3−/−
Control
Foxd1-Phd2−/−-Phd3−/−
ACTA2
CD31
e
Epo mRNA/18S
***
Col1a1 mRNA/18S
**
F4/80 mRNA/18S
*
Control
Phd2−/−
Phd3−/−
f
Cd31 mRNA/18S
*
Acta2 mRNA/18S
Lumen area (%)
**

demonstrated by RNA fluorescent *in situ* hybridization (data not shown), which is consistent with the findings in adult *Foxd1-Phd2*$^{-/-}$ mice.[26] Differences in *Acta2* mRNA expression levels were not observed. Altogether, our data demonstrate that the inactivation of both PHD2 and PHD3 in stromal cells resulted in interstitial HIF activation, which led to renal failure and was associated with juvenile lethality.

Combined loss of *Phd2* and *Phd3* in FOXD1 stroma results in reduced nephron formation

In mice, metanephric kidney development begins with the formation of the UB approximately at embryonic day (E) 10.5, which in turn induces the CM.[10,15] Because FOXD1 stromal cells, which surround the CM, are an important source of metanephric regulatory signals and have been shown to play a critical role in the maintenance and differentiation of epithelial progenitors,[14,16,17] we sought to determine the time point during development at which renal defects in *Foxd1-Phd2*$^{-/-}$*-Phd3*$^{-/-}$ mice became apparent. Therefore, we harvested kidneys from *Cre*$^{-}$ control, *Foxd1-Phd2*$^{-/-}$, and *Foxd1-Phd2*$^{-/-}$*-Phd3*$^{-/-}$-mice on P0, P7, and P14 and performed routine histologic analysis for morphologic assessment.

Foxd1-Phd2$^{-/-}$ kidneys were morphologically normal and could not be distinguished from control kidneys at either time point; however, kidneys from *Foxd1-Phd2*$^{-/-}$*-Phd3*$^{-/-}$ mutants were characterized by the presence of undifferentiated epithelial cells in the subcapsular cortex and a reduction in the number of differentiated proximal tubules (Figure 2). Periodic acid-Schiff staining, which identifies polysaccharides in the tubular basement and brush border membranes, demonstrated a lack of proximal tubule brush border staining in *Foxd1-Phd2*$^{-/-}$*-Phd3*$^{-/-}$ kidneys at P7 and P14 (Figure 2). In contrast, normal cortical periodic acid-Schiff staining patterns were found in *Cre*$^{-}$ control and *Foxd1-Phd2*$^{-/-}$ kidneys at P7, indicating that nephron formation was not affected by *Phd2* inactivation.

Toluidine blue staining demonstrated that the nephrogenic zone, which consists of the CM, ureteric tips, and early nephron structures such as renal vesicles, comma-shaped bodies, and S-shaped bodies, was morphologically similar between control, *Foxd1-Phd2*$^{-/-}$, and *Foxd1-Phd2*$^{-/-}$*-Phd3*$^{-/-}$ kidneys at P0. Differences in the size of the stromal cell compartment were not observed between control and *Foxd1-Phd2*$^{-/-}$*-Phd3*$^{-/-}$ kidneys (Supplementary Figure S3). Altogether, our findings suggest that the combined inactivation of *Phd2* and *Phd3* primarily affected the later stages of tubulogenesis, which became morphologically evident by P7 (Figure 2).

To further assess the *Foxd1-Phd2*$^{-/-}$*-Phd3*$^{-/-}$ phenotype, we performed lectin staining, IHC, and analyzed nephron segment–specific gene expression in whole-kidney homogenates using real-time PCR. The pattern of Lotus tetragonolobus lectin staining was consistent with a reduction in the number of mature proximal tubules (Figure 3a), which was statistically significant at P7 (156.8 $\pm$ 12.4 tubules/mm^2 in mutants vs. 300.7 $\pm$ 20.8 tubules/mm^2 in controls; n = 3 each; $P = 0.004$). Statistically significant differences were not observed at P0 (152.3 $\pm$ 15.0 tubules/mm^2 in mutants vs. 174.3 $\pm$ 14.8 tubules/mm^2 in *Cre*$^{-}$ controls; n = 3 each), supporting the notion that the combined inactivation of PHD2 and PHD3 affected postnatal nephron development, which terminates within the first week after birth in mice.[27,28] The expression of 2 additional proximal tubule maturation markers, megalin and cubilin, was also significantly decreased in *Foxd1-Phd2*$^{-/-}$*-Phd3*$^{-/-}$ mutants (Supplementary Figure S4). In contrast, the staining patterns and density of Tamm-Horsfall protein (uromodulin) expression, a marker of the thick ascending limb of the loop of Henle, and those of lectin Dolichos biflorus agglutinin, which identifies the collecting duct, were comparable between control and *Foxd1-Phd2*$^{-/-}$*-Phd3*$^{-/-}$ kidneys (Figure 3b). Morphologic findings were consistent with a significant decrease in *aquaporin1* and *sodium-phosphate cotransporter-2a* mRNA levels, whereas mRNA expression levels of the thick ascending limb of the loop of Henle gene *Nkcc2*, which encodes the Na-K-2Cl cotransporter 2; *transient receptor potential cation channel subfamily V member 5*, which is associated with the distal tubule; and collecting duct–specific *aquaporin 2* were not reduced. In contrast mRNA levels of *uromodulin*, *NaCl cotransporter, and sodium channel epithelial 1 alpha subunit* in mutants were significantly reduced compared with those in controls (Figure 3c). The reduction in the number of mature nephrons in *Foxd1-Phd2*$^{-/-}$*-Phd3*$^{-/-}$ mutants was associated with a decrease in the number of glomeruli at P7 (45.0 $\pm$ 2.5 glomeruli/mm^2 in mutants vs. 58.0 $\pm$ 4.1 glomeruli/mm^2 in controls; n = 5 and 4, respectively; $P < 0.05$; Figure 3d). In

Figure 1 | Combined inactivation of *prolyl-4-hydroxylase domain 2* (*Phd2*) and *Phd3* in forkhead box D1 (FOXD1) stromal cells results in renal failure. (**a**) Schematic illustrating the experimental approach and location of targeted sequences within the *Phd2* and *Phd3* floxed alleles. (**b**) Survival curve of *Cre*$^{-}$ littermate controls (*Foxd1*$^{+/+}$ *Phd2*$^{fl/fl}$ and *Foxd1*$^{+/+}$ *Phd2*$^{fl/fl}$ *Phd3*$^{fl/fl}$ mice) and *Foxd1-Phd2*$^{-/-}$ and *Foxd1-Phd2*$^{-/-}$*-Phd3*$^{-/-}$ mice. Kaplan-Meier curves were plotted and compared using the log-rank test (n > 10); ***$P < 0.001$. (**c**) Blood urea nitrogen (BUN) from *Cre*$^{-}$ littermate control and *Foxd1-Phd2*$^{-/-}$*-Phd3*$^{-/-}$ mice at postnatal day (P) 14 to P17 (n = 3 each). (**d**) Representative hematoxylin and eosin (H&E) images and immunostaining for alpha actin-2 (ACTA2) and cluster of differentiation (CD)31 of kidney sections from *Cre*$^{-}$ control and *Foxd1-Phd2*$^{-/-}$*-Phd3*$^{-/-}$ mice at P14 and P30. Asterisks indicate cysts, # indicates dilated vessels, yellow arrows indicate vascular walls, and blue arrows indicate glomeruli. Bar = 1 mm for whole-kidney cross-sections, 100 μm for high-power H&E images, and 50 μm for ACTA2-CD31 immunostaining. (**e,f**) *Erythropoietin* (*Epo*), *collagen type 1 alpha 1 (Col1a1),* and *F4/80* mRNA levels in *Cre*$^{-}$ littermate control and *Foxd1-Phd2*$^{-/-}$*-Phd3*$^{-/-}$ mutant kidneys at P14 (n = 8–10). Vascular lumina were quantified, and they are represented as total lumen area per tissue area (n = 3 each). Data are represented as mean $\pm$ SEM; 2-tailed Student's *t*-test; *$P < 0.05$, **$P < 0.01$, and ***$P < 0.001$. eGFP, enhanced green fluorescent protein. To optimize viewing of this image, please see the online version of this article at www.kidney-international.org.

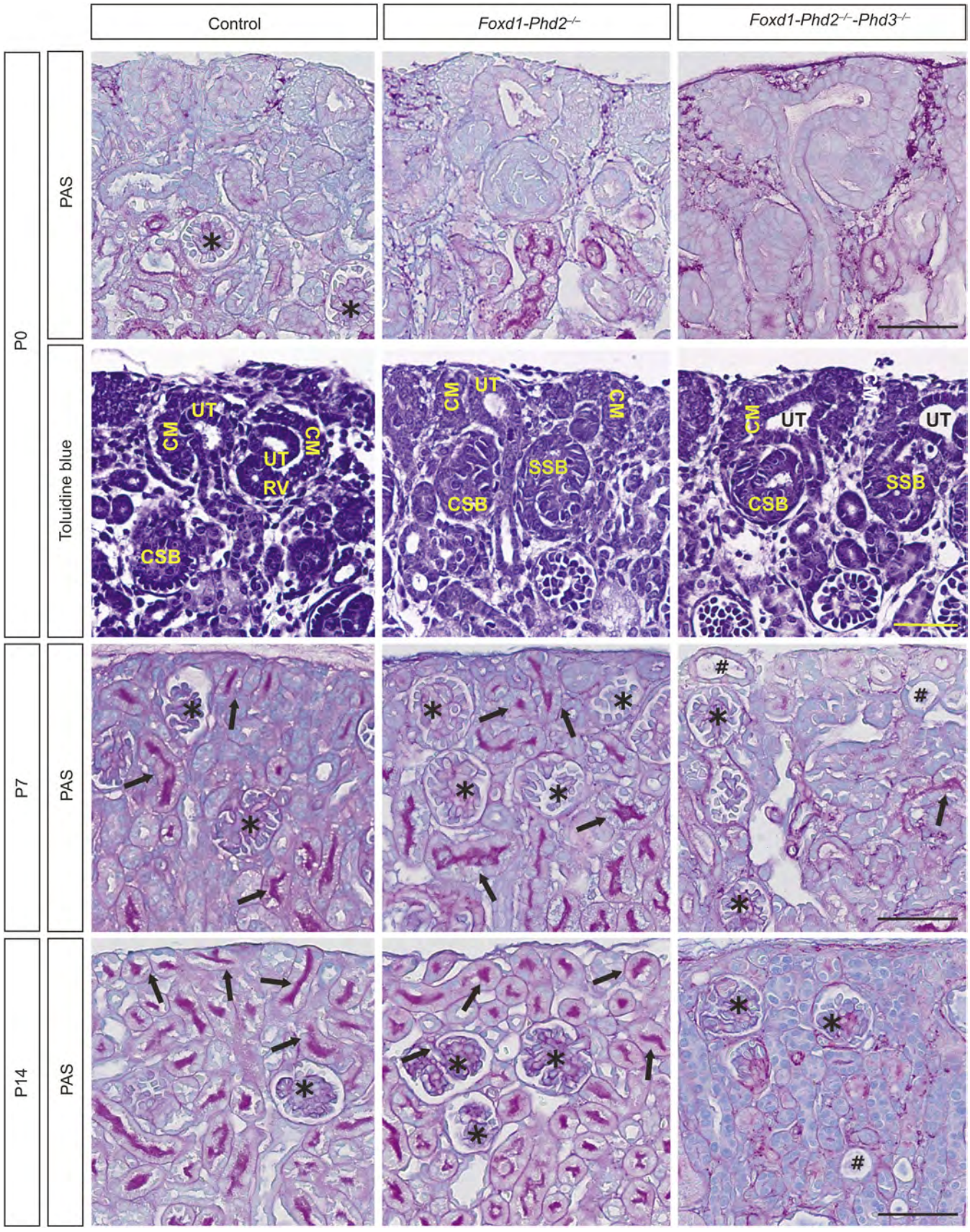
Control
Foxd1-Phd2-/-
Foxd1-Phd2-/--Phd3-/-
P0
P7
P14
PAS
Toluidine blue
UT
CM
RV
CSB
SSB

summary, our data suggest that the combined loss of PHD2 and PHD3 catalytic activity in FOXD1 stromal progenitors suppressed nephron formation, which in turn led to renal failure in juvenile mice.

Sine oculis–related homeobox 2–expressing progenitors are not reduced in *Foxd1-Phd2*$^{-/-}$*-Phd3*$^{-/-}$ kidneys

FOXD1 stroma–derived interstitial cells play a critical role in the maintenance and differentiation of renal epithelial progenitor cells, which are contained within the CM. The CM represents the induced mesenchyme and contains several layers of cells that express multiple transcription factors, including paired box 2, sine oculis–related homeobox 2 (SIX2), and spalt-like transcription factor 1, as well as several secreted molecules.[10,11] To better understand the pathogenesis of defective nephron formation in *Foxd1-Phd2*$^{-/-}$*-Phd3*$^{-/-}$ mice, we performed morphologic analyses and gene expression studies to assess for potential abnormalities in the nephrogenic zones of mutant kidneys. IHC analysis for SIX2, cytokeratin, spalt-like transcription factor 1, paired box 2, neural cell adhesion molecule 1, E-cadherin, and LIM homeobox protein 1 at E15.5 and P0 indicated that the CM volume was not reduced and that renal vesicle formation was not defective in *Foxd1-Phd2*$^{-/-}$*-Phd3*$^{-/-}$ mutants (Figure 4a and b). However, real-time PCR analysis at P0 demonstrated that *Six2, spalt-like transcription factor 1, and paired box 2* mRNA levels in whole-kidney homogenates from *Foxd1-Phd2*$^{-/-}$*-Phd3*$^{-/-}$ mice were significantly increased compared with *Cre*$^{-}$ control mice (approximately 1.8-, 1.5-, and 1.4-fold, respectively), suggesting a moderate expansion in the CM volume (Figure 4c). By P7, SIX2 expression, which is highly associated with the epithelial progenitor compartment, was no longer detectable in both control and *Foxd1-Phd2*$^{-/-}$*-Phd3*$^{-/-}$ kidneys (Figure 4a), indicating that reduced nephron formation in *Foxd1-Phd2*$^{-/-}$*-Phd3*$^{-/-}$mutants was not associated with the abnormal persistence of epithelial progenitor cells. Altogether, our data suggest that *Foxd1-Phd2*$^{-/-}$*-Phd3*$^{-/-}$ mutant mice were not characterized by major defects in prenatal nephrogenesis or the diminished presence of renal progenitors.

Reduced nephron formation in *Foxd1-Phd2*$^{-/-}$*-Phd3*$^{-/-}$ kidneys is dependent on the extent of stromal HIF activation

We previously showed that *Foxd1-Cre*–mediated inactivation of PHD2 in adult mice resulted in HIF-2 activation in a subset of renal interstitial cells. This was associated with increased *Epo* and *vascular endothelial growth factor* transcription and suggested that renal interstitial cells were heterogeneous with regard to their responsiveness to PHD2 inactivation.[26] Although HIF prolyl-4-hydroxylases regulate the activity of both HIF-1α and HIF-2α, HIF-1α was not detectable in adult *Foxd1-Phd2*$^{-/-}$ kidneys. To examine whether HIF-1α was expressed in the renal stroma during development, we performed IHC to investigate the cellular and spatial distribution of HIF-1α and HIF-2α in kidneys from newborn *Cre*$^{-}$ control, *Foxd1-Phd2*$^{-/-}$, and *Foxd1-Phd2*$^{-/-}$*-Phd3*$^{-/-}$ mice. In contrast to adults, nuclear HIF-1α staining was detectable in the cortex of both *Foxd1-Phd2*$^{-/-}$ and *Foxd1-Phd2*$^{-/-}$*-Phd3*$^{-/-}$ kidneys at P0 and was predominantly localized to the nephrogenic zone, whereas the majority of cortical HIF-2α–expressing cells were found in the subnephrogenic zone, suggesting a homolog-dependent spatial distribution pattern for HIF-α subunits in the developing cortical interstitium (Figure 5a). However, in the renal medulla, both HIF-1α– and HIF-2α–expressing interstitial cells were detected (data not shown). The spatial distribution of HIF-2α was consistent with that of *Epo* transcripts, which were not detected in the nephrogenic cortex using RNA fluorescent *in situ* hybridization (Figure 5b).

To determine whether abnormal nephron formation in *Foxd1-Phd2*$^{-/-}$*-Phd3*$^{-/-}$ mice is correlated with the degree of interstitial HIF activation, we determined the number of HIF-1α– and HIF-2α–expressing cells in *Cre*$^{-}$ control, *Foxd1-Phd2*$^{-/-}$, and *Foxd1-Phd2*$^{-/-}$*-Phd3*$^{-/-}$ kidneys. We found that compared with *Foxd1-Phd2*$^{-/-}$mice, the number of both HIF-1α– and HIF-2α–expressing stromal cells was significantly increased in *Foxd1-Phd2*$^{-/-}$*-Phd3*$^{-/-}$ kidneys (16.5 ± 3.3 cells/0.01 mm^2 vs. 6.5 ± 1.2 cells/0.01 mm^2 for HIF-1α and 3.32 ± 1.25 cells/0.01 mm^2 vs. 0.77 ± 0.14 cells/0.01 mm^2 for HIF-2α; $n = 3$ and 4, respectively; and $P < 0.01$ and $P < 0.05$, respectively; Figure 5a). The increased presence of HIF-α–expressing cells was also found in *Foxd1-von Hippel-Lindau (Vhl)*$^{-/-}$ mice, which are characterized by renal maturation defects similar to those observed in *Foxd1-Phd2*$^{-/-}$*-Phd3*$^{-/-}$mutants (Supplementary Figure S5).

Altogether, our data suggest that (i) HIF-1α and HIF-2α are differentially expressed in FOXD1 stroma–derived cells during kidney development, (ii) FOXD1 stroma–derived cells respond differentially to PHD2 inactivation, and (iii) the development of renal maturation defects is dependent on the extent of HIF activation in the renal stroma, namely the number of cells that express HIF-α.

Nephron formation defect in *Foxd1-Phd2*$^{-/-}$*-Phd3*$^{-/-}$ mice is dependent on HIF-2 activation

To examine the degree to which HIF-1 or HIF-2 signaling contributed to defective nephron formation in *Foxd1-Phd2*$^{-/-}$*-Phd3*$^{-/-}$ mice, we generated *Foxd1-Phd2*$^{-/-}$*-Phd3*$^{-/-}$*-Hif1a*$^{-/-}$

Figure 2 | Defective nephron formation in *Foxd1-Phd2*$^{-/-}$*-Phd3*$^{-/-}$ mice. Representative images of periodic acid-Schiff (PAS)–stained kidney sections from *Cre*$^{-}$ control (*Foxd1*$^{+/+}$ *Phd2*$^{fl/fl}$ *Phd3*$^{fl/fl}$ for postnatal day [P] 0 and *Foxd1*$^{+/+}$ *Phd2*$^{fl/fl}$ for P7 and P14), *Foxd1-Phd2*$^{-/-}$, and *Foxd1-Phd2*$^{-/-}$*-Phd3*$^{-/-}$ mice at P0, P7, and P14, and toluidine blue–stained kidney sections from P0 mice. Arrows indicate PAS-positive mature tubules, asterisks indicate glomeruli, and # indicates dilated tubules. Bar = 50 μm. CM, cap mesenchyme; CSB, comma-shaped body; *Foxd1*, *forkhead box D1*; *Phd*, *prolyl-4-hydroxylase domain*; RV, renal vesicle; SSB, S-shaped body; UT, ureteric tip. To optimize viewing of this image, please see the online version of this article at www.kidney-international.org.

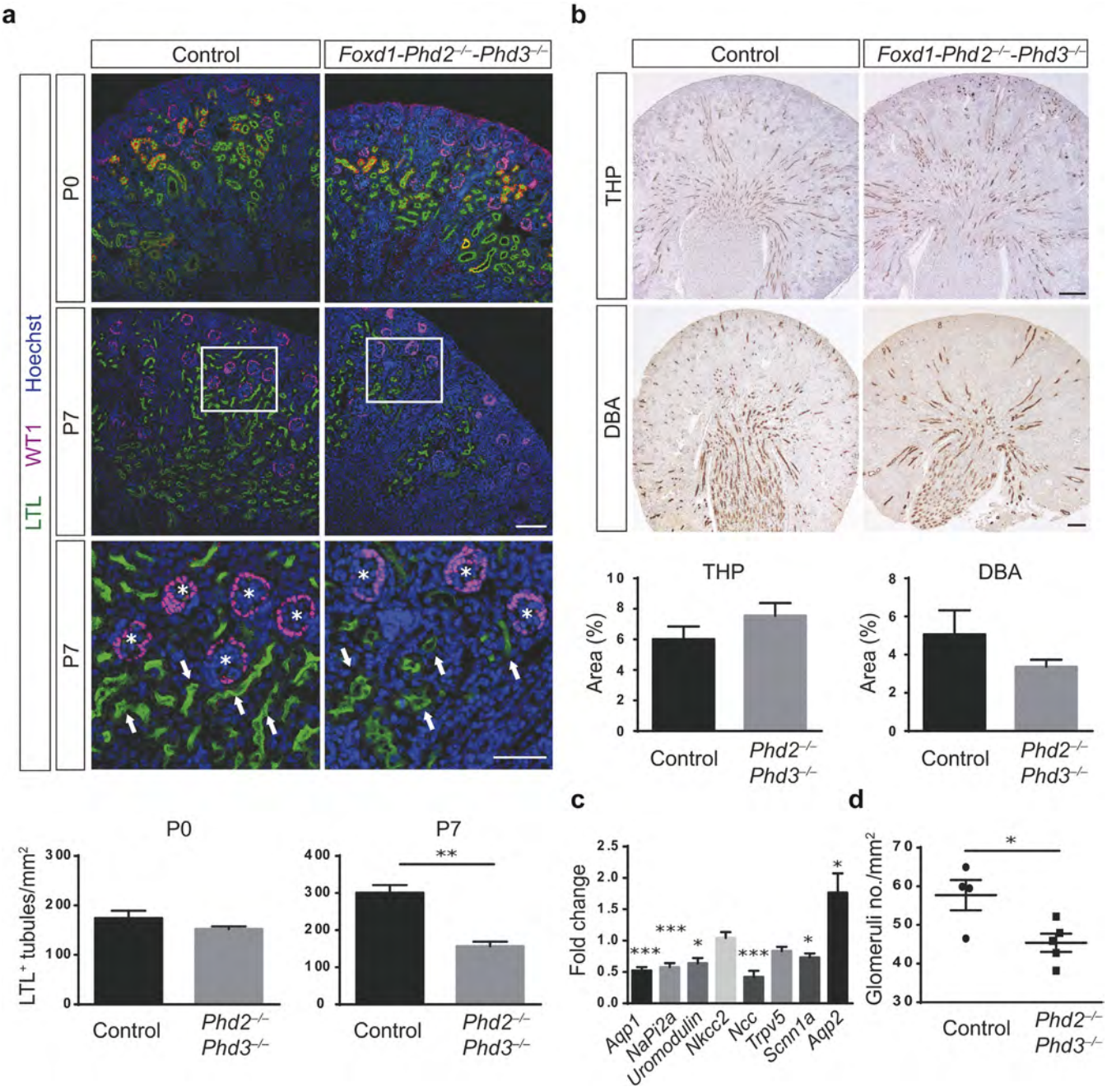

Figure 3 | Combined inactivation of *prolyl-4-hydroxylase domain 2* (*Phd2*) and *Phd3* in forkhead box D1 (FOXD1) stromal cells reduces nephron formation. (**a**) Representative images of Lotus tetragonolobus lectin (LTL) staining (green) and immunohistochemistry (IHC) staining for Wilms' tumor 1 (WT1) (pink); kidney sections were obtained from *Cre*$^{-}$ littermate controls or *Foxd1-Phd2*$^{-/-}$*-Phd3*$^{-/-}$ mutants at postnatal day (P) 0 or P7. Nuclei were stained with Hoechst dye. Arrows indicate proximal tubules and asterisks indicate glomeruli. Bar = 100 μm (top and middle panels) and 50 μm (bottom panel). LTL^{+} tubules were quantified (n = 3 each) at P0 and P7. (**b**) Representative images of IHC staining for Tamm-Horsfall protein (THP) and Dolichos biflorus agglutinin (DBA) lectin staining of kidney sections from *Cre*$^{-}$ littermate controls and *Foxd1-Phd2*$^{-/-}$*-Phd3*$^{-/-}$ mice at P7. THP^{+} and DBA^{+} tubules were quantified (n = 3–5). Bar = 200 μm. (**c**) Fold changes in mRNA expression levels of nephron segment–specific genes in total kidney homogenates from *Foxd1-Phd2*$^{-/-}$*-Phd3*$^{-/-}$ mutants compared with *Cre*$^{-}$ littermate controls (n = 8 each). (**d**) Quantification of glomerular numbers. Data given as the number of glomeruli per mm^2 (n = 4–5). Data are represented as mean ± SEM; 2-tailed Student's *t*-test, *$P < 0.05$, **$P < 0.01$, and ***$P < 0.001$. *Aqp1*, *aquaporin 1*; *Aqp2*, *aquaporin 2*; *NaPi2a*, *sodium-phosphate cotransporter-2a*; *Ncc*, *NaCl cotransporter*; *Nkcc2*, *Na-K-2Cl cotransporter*; *Scnn1a*, *sodium channel epithelial 1 alpha subunit*; *Trpv5*, *transient receptor potential cation channel subfamily V member 5*. To optimize viewing of this image, please see the online version of this article at www.kidney-international.org.

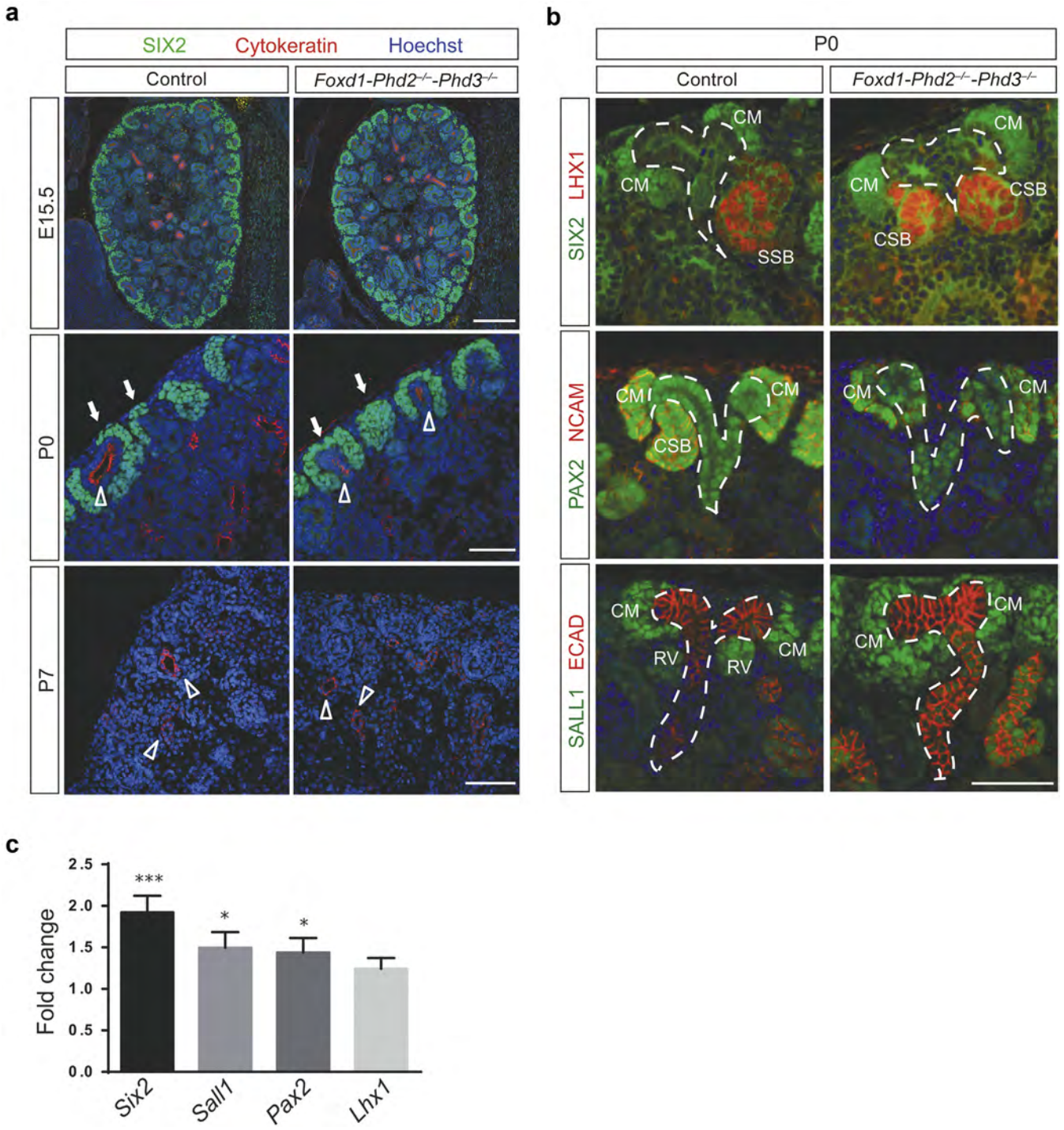

Figure 4 | Nephron progenitors are not decreased in *Foxd1-Phd2*$^{-/-}$*-Phd3*$^{-/-}$ kidneys. (**a**) Representative images of immunohistochemistry (IHC) staining of formalin-fixed paraffin-embedded kidney sections for the nephron progenitor markers sine oculis-related homeobox 2 (SIX2; green) and ureteric bud (UB) marker pan-cytokeratin (red); results for *Cre*$^{-}$ littermate controls and *Foxd1-Phd2*$^{-/-}$*-Phd3*$^{-/-}$ mutants at embryonic day (E) 15.5, postnatal day (P) 0, or P7 are shown. Nuclei were stained with Hoechst dye. Bar = 200 μm (E15.5) and 50 μm (P0 and P7). Arrows indicate cap mesenchyme (CM) and open arrowheads indicate UB. (**b**) Representative images of SIX2 (green) and LIM homeobox protein 1 (LXH1; red) (top panels), paired box 2 (PAX2; green) and neural cell adhesion molecule 1 (NCAM; red) (middle panels), and spalt-like transcription factor 1 (SALL1; green) and E-cadherin (ECAD; red) (bottom panels) IHC staining of formalin-fixed paraffin-embedded kidney sections from *Cre*$^{-}$ littermate control and *Foxd1-Phd2*$^{-/-}$*-Phd3*$^{-/-}$ mice at P0. Nuclei were stained with Hoechst dye. Ureteric trees are outlined by dashed white lines and CM, renal vesicle (RV), comma-shaped body (CSB), and S-shaped body (SSB) are annotated. Bar = 50 μm. (**c**) Fold changes in *Six2*, *Sall1*, *Pax2,* and *Lhx1* mRNA expression levels in total kidney homogenates from *Foxd1-Phd2*$^{-/-}$*-Phd3*$^{-/-}$ mutants at P0 compared with *Cre*$^{-}$ littermate controls (n = 12 for control and n = 10 for mutants). Data are represented as mean ± SEM; 2-tailed Student's *t*-test; ***$P < 0.001$ and *$P < 0.05$. *Foxd1, forkhead box D1*; *Phd, prolyl-4-hydroxylase domain*. To optimize viewing of this image, please see the online version of this article at www.kidney-international.org.

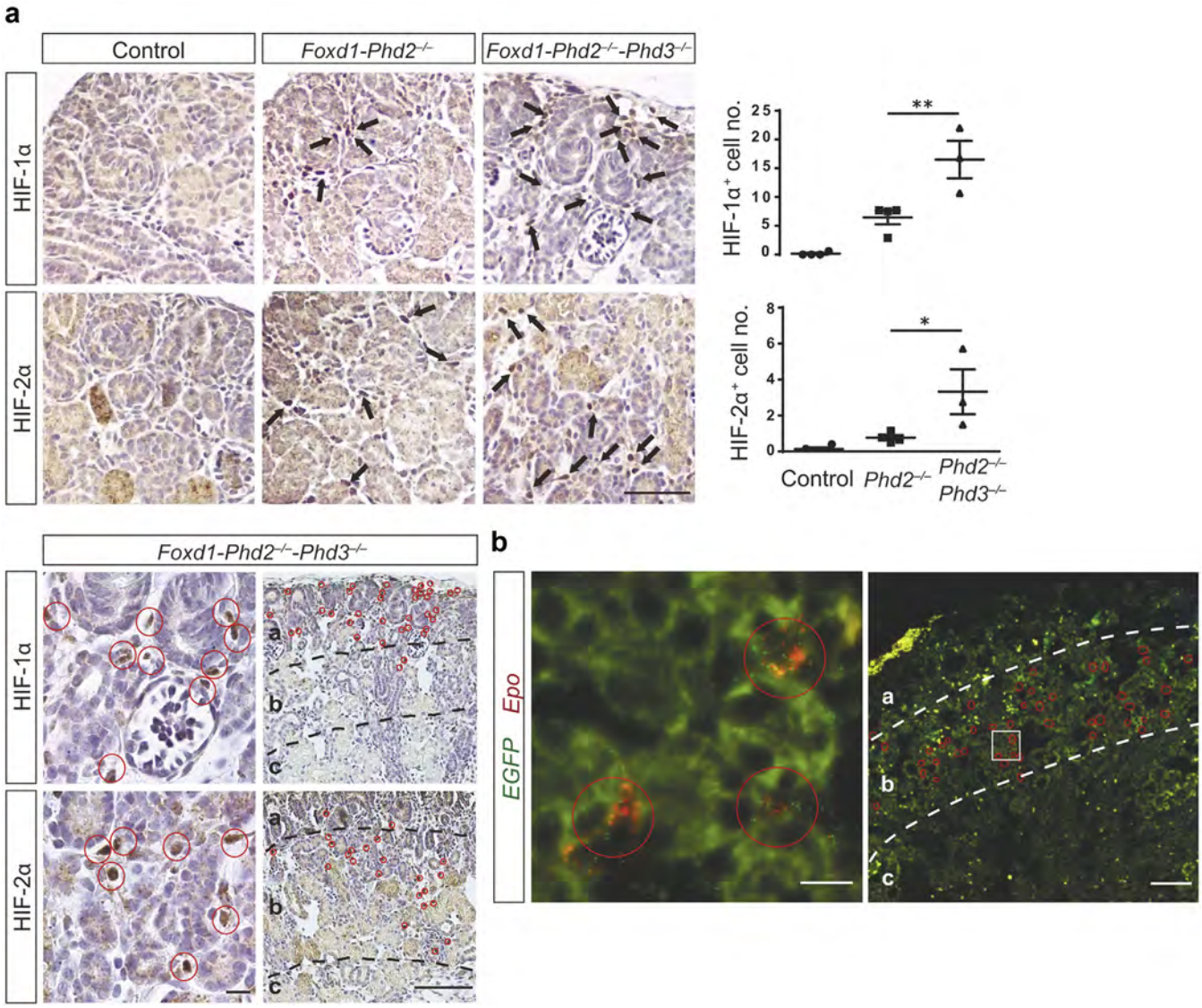

Figure 5 | *Prolyl-4-hydroxylase domain 3* (*Phd3*) inactivation in *Phd2*$^{-/-}$ forkhead box D1 (FOXD1) stromal cells increases the number of hypoxia-inducible factor (HIF)-α–expressing cells. (**a**) Representative images of HIF-1α and HIF-2α immunohistochemistry (IHC) staining of formalin-fixed, paraffin-embedded kidney sections from *Cre*$^{-}$ control (*Foxd1*$^{+/+}$ *Phd2*$^{fl/fl}$ *and Foxd1*$^{+/+}$ *Phd2*$^{fl/fl}$ *Phd3*$^{fl/fl}$), *Foxd1-Phd2*$^{-/-}$, and *Foxd1-Phd2*$^{-/-}$*-Phd3*$^{-/-}$ mice at postnatal day 0 (n = 3–4). Arrows indicate HIF-α^{+} cells. To facilitate visualization and provide an overview of HIF-α^{+} cell distribution at low magnification, HIF-α^{+} cells were annotated with red circles (bottom panels). The extent of stromal HIF activation is expressed as the HIF-α^{+} cell number per 0.01 mm^2. The *Cre*$^{-}$ control group comprised 1 *Foxd1*$^{+/+}$ *Phd2*$^{fl/fl}$ and 3 *Foxd1*$^{+/+}$ *Phd2*$^{fl/fl}$ *Phd3*$^{fl/fl}$ mice. Data are represented as mean ± SEM and were analyzed using 1-way analysis of variance; $^{**}P < 0.01$. Bar = 50 μm (top panels), 10 μm (high-magnification images, bottom left panels), and 100 μm (low-magnification images, bottom, right panels). (**b**) Images illustrate the distribution of *erythropoietin* (*Epo*)$^{+}$ cells in *Foxd1-mT/mG-Phd2*$^{-/-}$*-Phd3*$^{-/-}$ kidneys using RNA fluorescent *in situ* hybridization. To facilitate visualization and provide an overview of *Epo*$^{+}$ cell distribution at a low magnification, *Epo*$^{+}$ cells were annotated with red circles. *Epo* transcripts were detected by red fluorescence, and *enhanced green fluorescent protein* (*EGFP*) transcripts (cells with a history of *Foxd1-cre* expression) were detected by green fluorescence (left panel). Bar = 10 μm (left) and 100 μm (right). Labeling of low-magnification images in (**a**) and (**b**): *a*, superficial cortex with nephrogenic zone; *b*, deeper cortex; and *c*, medulla. To optimize viewing of this image, please see the online version of this article at www.kidney-international.org.

and *Foxd1-Phd2*$^{-/-}$*-Phd3*$^{-/-}$*-Hif2a*$^{-/-}$ triple-mutant mice in which PHD2 and PHD3 were inactivated together with either HIF-1α or HIF-2α (recombination for all targeted 2-lox alleles was equally efficient in *Foxd1-Phd2*$^{-/-}$*-Phd3*$^{-/-}$*-Hif1a*$^{-/-}$ and *Foxd1-Phd2*$^{-/-}$*-Phd3*$^{-/-}$*-Hif2a*$^{-/-}$mutants [Supplementary Figure S6]). *Foxd1-Phd2*$^{-/-}$*-Phd3*$^{-/-}$*-Hif1a*$^{-/-}$ mutants developed nephron formation defects similar to those observed in *Foxd1-Phd2*$^{-/-}$*-Phd3*$^{-/-}$ mice and were characterized by small kidneys and abnormal periodic acid-Schiff, Lotus tetragonolobus lectin, and Tamm-Horsfall protein staining patterns (Figure 6a; Supplementary Figure S7). Morphologic abnormalities were consistent with the reduced expression of

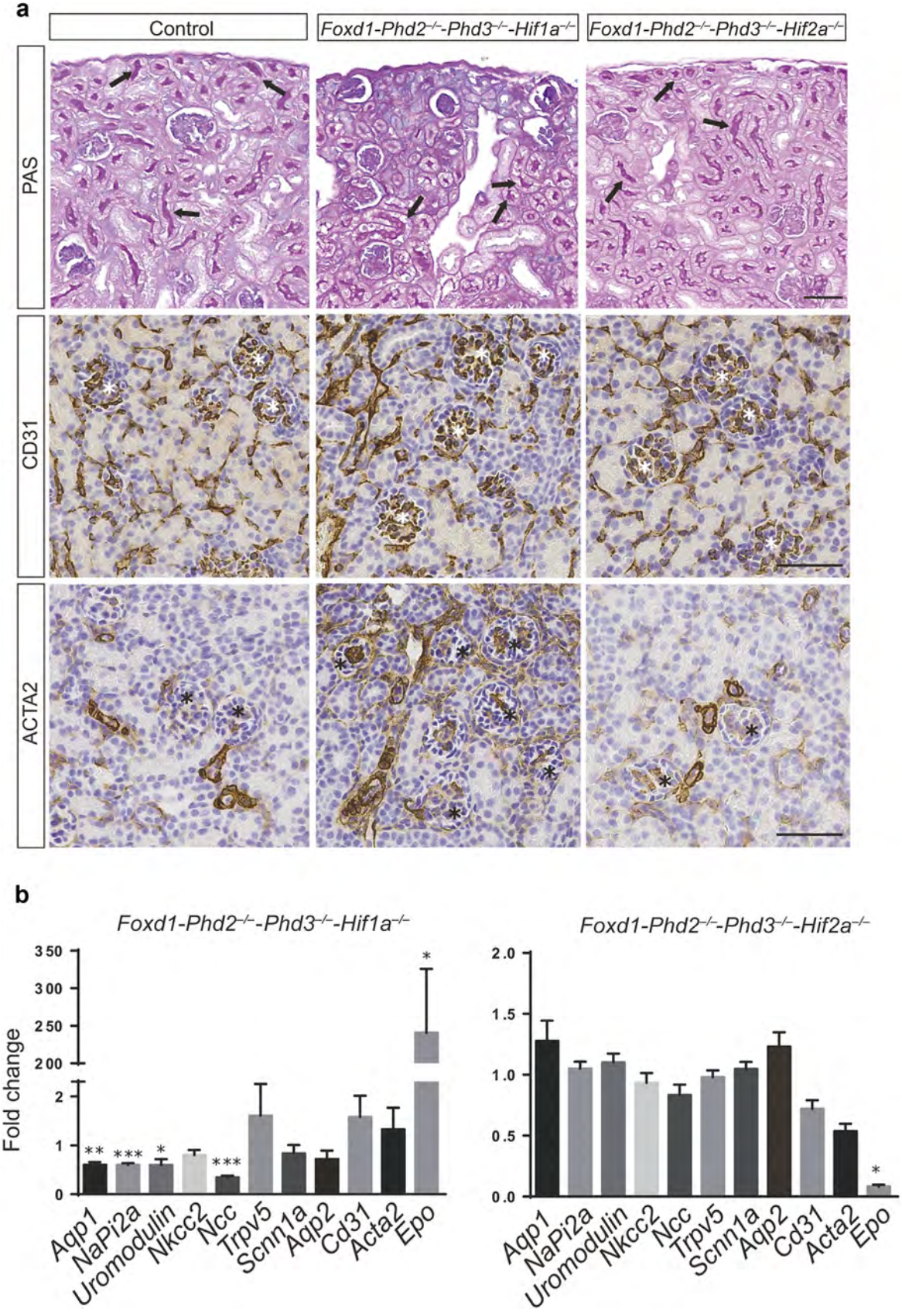
a
Control
Foxd1-Phd2-/--Phd3-/--Hif1a-/-
Foxd1-Phd2-/--Phd3-/--Hif2a-/-
PAS
CD31
ACTA2
b
Foxd1-Phd2-/--Phd3-/--Hif1a-/-
Foxd1-Phd2-/--Phd3-/--Hif2a-/-
Fold change
350
300
250
200
2
1
0
2.0
1.5
1.0
0.5
0.0
**
***
*
***
*
Aqp1
NaPi2a
Uromodulin
Nkcc2
Ncc
Trpv5
Scnn1a
Aqp2
Cd31
Acta2
Epo

mRNAs encoding nephron segment–specific markers (Figure 6b). Furthermore, nephron formation defects in *Foxd1-Phd2*$^{-/-}$*-Phd3*$^{-/-}$*-Hif1a*$^{-/-}$ mutants were associated with enhanced ACTA2 staining in glomeruli and renal interstitium (Figure 6a). In contrast, *Foxd1-Phd2*$^{-/-}$*-Phd3*$^{-/-}$*-Hif2a*$^{-/-}$ triple-mutant mice survived to adulthood, had normal-sized kidneys, and did not display any developmental defects or differences in the expression of mRNAs encoding epithelial or vascular markers compared with *Cre*$^{-}$ littermate controls. However, *Epo* mRNA levels were severely reduced in *Foxd1-Phd2*$^{-/-}$*-Phd3*$^{-/-}$*-Hif2a*$^{-/-}$ kidneys, which is an expected finding because renal *Epo* transcription is HIF-2 dependent (Figure 6b).[29] *Foxd1-Cre*–mediated deletion of *Hif1a* or *Hif2a* alone did not result in renal maturation defects, although smaller body and kidney weights were observed in *Foxd1-Hif1a*$^{-/-}$ mice at P14 (Supplementary Figure S8). Our data demonstrate that the inactivation of HIF-2α but not HIF-1α in FOXD1 stroma was sufficient to restore normal nephron formation in *Foxd1-Phd2*$^{-/-}$*-Phd3*$^{-/-}$ mutant mice.

DISCUSSION

Here we developed several genetic models to investigate the role of individual HIF prolyl-4-hydroxylases in renal homeostasis. We demonstrate that the HIF oxygen–sensing pathway in FOXD1 stroma has a crucial function during nephrogenesis and that the ability to hydroxylate HIF-2α via PHD2 and PHD3 is required for normal nephron formation. Our data suggest that PHD2 is indispensable for normal physiological control of interstitial HIF activity during renal development because it functions as the main HIF prolyl-4-hydroxylase in FOXD1 stroma–derived interstitial cells, whereas PHD3 is dispensable in the presence of PHD2 but becomes rate limiting when PHD2 catalytic activity is inhibited or absent (Figure 7). Furthermore, we provide evidence for a distinct and nonoverlapping spatial distribution of interstitial HIF-1α and HIF-2α during development and propose that the physiological control of HIF-2 signaling in the renal stroma is critically important for normal kidney development.

Experimental intrauterine hypoxia has been shown to affect kidney development and postnatal renal function at multiple levels and is associated with low kidney weight at birth, low nephron endowment, reduced glomerular number, and abnormal intrarenal vascular regulation.[7,30–33] Our genetic studies establish that the stromal PHD-HIF axis is a critical component of the renal hypoxia response system that regulates late nephrogenesis in a HIF-2–dependent manner. However, the developmental role of individual HIF transcription factors in other cell types is less clear. Although mice with germline HIF-1α deletion die *in utero* between E9.5 and E11, precluding studies of renal development,[34,35] hypoxia and the widespread induction of HIF-1 signaling has been shown to restrict branching morphogenesis *in vitro*, possibly through the release of antibranching factors.[33] Genetic HIF activation in UB cells specifically increased kidney size, the number of glomeruli, and very modestly enhanced UB branching, whereas UB-directed HIF-1α inactivation had the opposite effect, suggesting cell type–dependent functions of renal HIF signaling during development.[33] In contrast, renal development was reported to be normal in a mixed-background strain of mice with germline HIF-2α inactivation.[20] Normal kidney development was also reported in a genetic model of renal epithelial HIF activation generated by *Vhl* gene deletion in SIX2^{+} epithelial progenitor cells.[36] However, *Six2-Cre-Vhl* mutant mice developed renal failure as adults. Whether nephron endowment was affected in this model is unclear. Furthermore, defects in renal development were not reported in endothelial cell–specific HIF knockout models.[37] These studies, together with our data, support the concept of cell type–dependent roles of individual HIF transcription factors in renal organogenesis.

Our studies have implications for human biology that reach beyond gestational hypoxia as PHD inhibitors are currently in clinical development for renal anemia.[38] Some of the inhibiting compounds display a preferential activity for certain PHDs; however, the degree to which individual compounds impact nephrogenesis will have to be examined.[21]

Although the *Foxd1-Phd2*$^{-/-}$*-Phd3*$^{-/-}$ mutant phenotype is complex and involves multiple cell types, our studies indicate dependence on the extent of stromal HIF activation, namely the number/density of HIF-α–expressing cells in the kidney (Figure 7). Although PHD2 is the main regulator of HIF in many cell types, PHD1 and PHD3 dioxygenases play a significant role in controlling HIF activity in a context- and cell type–dependent manner.[3,39–41] Our genetic data establish that PHD2 catalysis alone is sufficient for HIF-α degradation in FOXD1 stroma–derived interstitial cells because the individual or combined inactivation of *Phd1* and *Phd3* does not

Figure 6 | Nephron formation defects in *Foxd1-Phd2*$^{-/-}$*-Phd3*$^{-/-}$ mice require hypoxia-inducible factor (HIF)-2α. (**a**) Representative images of periodic acid-Schiff (PAS)–stained kidney sections (top) and cluster of differentiation (CD)31 and ACTA2 immunohistochemistry (IHC) staining (middle and lower panels) for *Cre*$^{-}$ control (*Foxd1*$^{+/+}$ *Phd2*$^{fl/fl}$ *Phd3*$^{fl/fl}$ *Hif2a*$^{fl/fl}$), *Foxd1-Phd2*$^{-/-}$*-Phd3*$^{-/-}$*-Hif1a*$^{-/-}$, and *Foxd1-Phd2*$^{-/-}$*-Phd3*$^{-/-}$*-Hif2a*$^{-/-}$mutant kidneys at postnatal day 14. Asterisks indicate glomeruli, and arrows indicate renal tubules with PAS-positive brush borders. Bar = 50 μm. (**b**) mRNA expression levels of *erythropoietin* (*Epo*), nephron segment–specific, and vascular markers in whole-kidney homogenates from *Foxd1-Phd2*$^{-/-}$*-Phd3*$^{-/-}$*-Hif1a*$^{-/-}$, and *Foxd1-Phd2*$^{-/-}$*-Phd3*$^{-/-}$*-Hif2a*$^{-/-}$ compared with those from *Cre*$^{-}$ controls (n = 4 for *Foxd1*$^{+/+}$ *Phd2*$^{fl/fl}$ *Phd3*$^{fl/fl}$ *Hif2a*$^{fl/fl}$ control mice; n = 3 for *Foxd1-Phd2*$^{-/-}$*-Phd3*$^{-/-}$*-Hif1a*$^{-/-}$ mutants; n = 5 each for *Foxd1-Phd2*$^{-/-}$*-Phd3*$^{-/-}$*-Hif2a*$^{-/-}$ mice). Data are represented as mean ± SEM; 2-tailed Student's *t*-test; *$P < 0.05$, **$P < 0.01$, and ***$P < 0.001$. *Acta2, alpha actin-2*; *Aqp1, aquaporin 1*; *Aqp2, aquaporin 2*; *Foxd1, forkhead box D1*; *NaPi2a, sodium-phosphate cotransporter-2a*; *Ncc, NaCl cotransporter*; *Nkcc2, Na-K-2Cl cotransporter*; *Phd, prolyl-4-hydroxylase domain*; *Scnn1a, sodium channel epithelial 1 alpha subunit*; *Trpv5, transient receptor potential cation channel subfamily V member 5*. To optimize viewing of this image, please see the online version of this article at www.kidney-international.org.

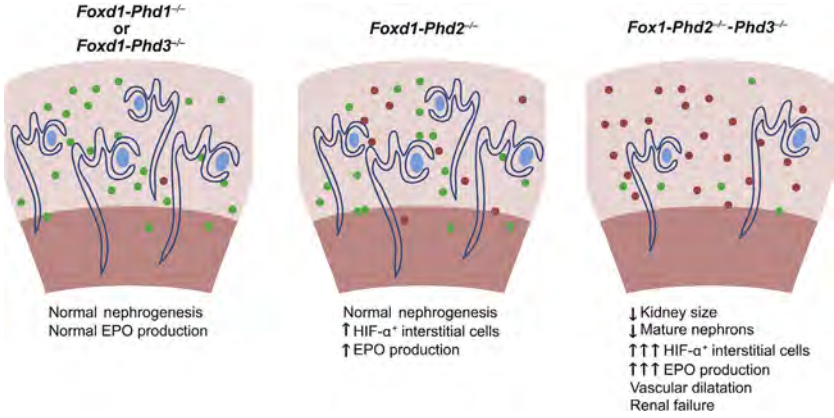

Figure 7 | Schematic depicting the role of prolyl-4-hydroxylase domain (PHD) dioxygenases in renal development. Hypoxia-inducible factor (HIF)-α^+ stromal cells are shown as red-filled circles; green-filled circles indicate targeted stromal cells where HIF-α was not detected. Normal erythropoietin (EPO) production in *Foxd1-Phd1*$^{-/-}$ or *Foxd1-Phd3*$^{-/-}$ mutant mice is indicated by a single red-filled circle.

result in detectable HIF-α stabilization. We also establish that PHD3, but not PHD1 (data not shown), is capable of suppressing HIF-α stabilization in a large subpopulation of *Phd2*$^{-/-}$ interstitial cells because *Foxd1-Phd2*$^{-/-}$*-Phd3*$^{-/-}$ mutants were characterized by a significant increase in the number of stromal cells with stabilized HIF-α compared with *Foxd1-Phd2*$^{-/-}$ mutants. As previously suggested, the differential sensitivity of the renal stroma to genetic *Phd2* deletion may be due to differences in PHD3 expression levels,[26] which could indicate that renal interstitial cells display differential responsiveness to hypoxia.[39,41]

In summary, our genetic studies establish a critical role of stromal HIF oxygen sensing in nephrogenesis. Our findings provide a strong rationale for further investigations of oxygen-regulated signals that control intercellular crosstalk during renal development and have implications for clinical studies that investigate the therapeutic potential of PHD inhibitors in humans.

MATERIALS AND METHODS

Generation and genotyping of mice and animal procedures

The generation and genotyping of mice with floxed alleles for *Phd1* (*Egln2*), *Phd2* (*Egln1*), *Phd3* (*Egln3*), *Hif1a*, and *Hif2a* (*Epas1*) has been described elsewhere.[42–44] *Foxd1-Phd2*$^{-/-}$*-Phd3*$^{-/-}$ mice were generated by breeding *Foxd1*$^{cre/+}$*Phd2*$^{fl/+}$ *Phd3*$^{fl/fl}$ mice with *Cre*-negative *Foxd1*$^{+/+}$*Phd2*$^{fl/fl}$ *Phd3*$^{fl/fl}$ mice. Only *Cre*$^{-}$ littermates served as controls. Details regarding animal studies can be found in the Supplementary Materials and Methods.

RNA analysis and IHC

Technical details can be found in the Supplementary Materials and Methods.

Statistics

Data are reported as mean ± SEM. Statistical analyses were performed using Prism 6 software (GraphPad Software Inc., La Jolla, CA), Student's *t*-test, or 1-way analysis of variance with Tukey's *post hoc* analysis. The survival curve was analyzed using the Kaplan-Meier method, and groups were compared using the log-rank test. *P* values of <0.05 were considered to be statistically significant.

Study approval and ethical permits

All procedures involving mice were performed in accordance with the National Institutes of Health guidelines for the use and care of live animals, and the procedures were approved by the Vanderbilt University Institutional Animal Care and Use Committee.

DISCLOSURE

VHH serves on the Scientific Advisory Board of Akebia Therapeutics, a company that develops prolyl-4-hydroxylase inhibitors for the treatment of anemia. All the other authors declared no competing interests.

ACKNOWLEDGMENTS

VHH is supported by the Krick-Brooks chair in Nephrology, NIH grants R01-DK101791 and R01-DK081646, a Department of Veterans Affairs Merit Award (1I01BX002348), and NIDDK Diabetic Complications Consortium (U24-DK076169). Additional support was provided by Vanderbilt's Diabetes Research and Training Center (P30-DK20593). Financial support for this work was also provided by the NIDDK Diabetic Complications Consortium (www.diacomp.org), grant U24-DK076169. The authors wish to thank Peter Ratcliffe and Tammie Bishop, University of Oxford for generously providing the PM8 HIF2α antibody. Whole-slide imaging was performed at the Digital Histology Shared Resource at Vanderbilt University Medical Center.

AUTHORS CONTRIBUTIONS

HK and VHH conceived and designed the research studies, analyzed and interpreted the data, drafted the manuscript, and prepared the figures. HK, JL, AAU, MB, KI, MR, and OL performed the experiments and acquired and analyzed the data. SZ provided conceptual input and helped in the interpretation of the data.

SUPPLEMENTARY MATERIAL

Table S1. Body and kidney weights in *Foxd1-Phd2*$^{-/-}$ and *Foxd1-Phd2*$^{-/-}$*Phd3*$^{-/-}$ mutants. Body and kidney weights of *Foxd1-Phd2*$^{-/-}$ and *Foxd1-Phd2*$^{-/-}$*-Phd3*$^{-/-}$ mice and their respective *Cre*$^{-}$ littermate controls at postnatal day (P) 0, P7, and P14. Data represent mean ±

SEM and were analyzed using the 2-tailed Student's *t*-test. *Foxd1, forkhead box D1*; *Phd*, *prolyl-4-hydroxylase domain*.

Figure S1. *Phd1*, *Phd2,* and *Phd3* expressions in forkhead box D1 (FOXD1) lineage cells. Representative RNA fluorescent *in situ* hybridization (RNA-FISH) images detecting *Phd1*, *Phd2*, and *Phd3* in formalin-fixed paraffin-embedded kidney sections from *Foxd1-mT/mG* mice at postnatal day (P) 0. Bar = 10 μm. *Enhanced green fluorescent protein* (*EGFP)* transcripts were detected by green fluorescence and surrounded the ureteric tree (depicted by white dashed lines), whereas *Phd1*, *Phd2,* and *Phd3* transcripts were detected by red fluorescence. Arrows indicate *EGFP-Phd* double-positive cells. *Phd*, *prolyl-4-hydroxylase domain*.

Figure S2. Combined inactivation of *Phd2* and *Phd3* in forkhead box D1 (FOXD1) stroma results in vascular dilatations. Representative images of alpha actin-2 (ACTA2) immunohistochemistry (IHC) staining of kidney tissue sections from Cre^- control and *Foxd1-Phd2*$^{-/-}$*-Phd3*$^{-/-}$ mutants at postnatal day (P) 7 and P14. Asterisks indicate glomeruli, red arrows indicate interlobular arteries, and black arrows indicate afferent arterioles. Bar = 50 μm. *Phd*, *prolyl-4-hydroxylase domain*.

Figure S3. Forkhead box D1 (FOXD1) lineage–derived cells are not increased in *Foxd1-Phd2*$^{-/-}$*-Phd3*$^{-/-}$ mouse kidneys. Representative images of RNA fluorescent *in situ* hybridization (RNA-FISH) detecting *enhanced green fluorescent protein* (*EGFP)* expression in formalin-fixed paraffin-embedded kidney sections from *Foxd1-mT/mG* control or *Foxd1-mT/mG-Phd2*$^{-/-}$*-Phd3*$^{-/-}$ mice at postnatal day (P) 0. Bar = 50 μm. Ureteric trees are outlined by dashed white lines. $EGFP^+$ cells were detected using green fluorescence, and $EGFP^+$ areas were quantified and expressed as %/high-power field (HPF; n = 3 each). Data are represented as mean ± SEM; 2-tailed Student's *t*-test; NS statistically not significant. Arrows indicate $EGFP^+$ cells. *Phd*, *prolyl-4-hydroxylase domain*.

Figure S4. *Phd2* and *Phd3* inactivation in forkhead box D1 (FOXD1) stroma reduces mature nephron formation. (**A**) Shown are representative images of immunohistochemistry (IHC) for megalin and cubilin using formalin-fixed paraffin-embedded kidney sections from Cre^- littermate control and *Foxd1-Phd2*$^{-/-}$*-Phd3*$^{-/-}$ mice at postnatal day (P) 7. Bar = 100 μm. (**B**) Quantification of megalin$^+$ and cubilin$^+$ tubules expressed as number of positively stained tubules per 0.1-mm^2 section area or percentage of positively stained area/high-power field (n = 3–5). Data are represented as mean ± SEM; 2-tailed Student's *t*-test, $^*P < 0.05$. *Phd*, *prolyl-4-hydroxylase domain*.

Figure S5. Inactivation of *von Hippel-Lindau* (*Vhl)* in forkhead box D1 (FOXD1) stromal cells results in juvenile lethality and defects in renal development. Representative images of periodic acid-Schiff (PAS)–stained kidney sections (top), and hypoxia-inducible factor (HIF)-1α (middle), and HIF-2α immunohistochemistry (IHC) staining (bottom) for Cre^- littermate control or *Foxd1-Vhl*$^{-/-}$ mice at postnatal day (P) 14. Bar = 100 μm for PAS-stained sections and 50 μm for HIF-stained sections. Asterisks indicate glomeruli, and arrows indicate renal tubules with PAS-positive brush borders (top panels) or HIF-1α$^+$ or HIF-2α$^+$ cells (lower 4 panels). *Phd*, *prolyl-4-hydroxylase domain*.

Figure S6. Recombination efficiency of targeted alleles in *Foxd1-Phd2*$^{-/-}$*-Phd3*$^{-/-}$*-Hif1a*$^{-/-}$and *Foxd1-Phd2*$^{-/-}$*-Phd3*$^{-/-}$*-Hif2a*$^{-/-}$ mutant mice. Genomic polymerase chain reaction (PCR) analysis of DNA isolated from kidneys of *Foxd1*$^{cre/+}$ *Phd2*$^{fl/fl}$ *Phd3*$^{fl/fl}$, *Foxd1*$^{cre/+}$ *Phd2*$^{fl/fl}$ *Phd3*$^{fl/fl}$ *Hif1a*$^{fl/fl}$, *Foxd1*$^{cre/+}$ *Phd2*$^{fl/fl}$ *Phd3*$^{fl/fl}$ *Hif2a*$^{fl/fl}$, and *Foxd1*$^{+/+}$ *Phd2*$^{fl/fl}$ *Phd3*$^{fl/fl}$ *Hif2a*$^{fl/fl}$ control mice (Cre^-). Two *Hif2a* wild-type (WT) alleles of different sizes were detected owing to polymorphism in the amplified regions of *Hif2a,* as previously described.[1] (This reference number refers to the bibliography in the Supplementary Material.) 1-lox indicates the recombined allele; 2-lox indicates the non-recombined conditional allele. *Foxd1*, *forkhead box D1*; HIF, hypoxia-inducible factor; *Phd*, *prolyl-4-hydroxylase domain*.

Figure S7. Renal maturation defects in *Foxd1-Phd2*$^{-/-}$*-Phd3*$^{-/-}$ mice do not require hypoxia-inducible factor (HIF)-1. Representative images of Lotus tetragonolobus lectin (LTL) staining (green fluorescent signal), immunohistochemistry (IHC) staining for Tamm-Horsfall protein (THP), and Dolichos biflorus agglutinin (DBA) staining of formalin-fixed paraffin-embedded kidney sections from Cre^- control or *Foxd1-Phd2*$^{-/-}$*-Phd3*$^{-/-}$*-Hif1a*$^{-/-}$ mice at postnatal day (P) 14. White arrows indicate LTL$^+$ tubules; black arrows indicate THP$^+$ or DBA$^+$ tubules. Bar = 100 μm for LTL-stained sections and 200 μm for THP IHC and DBA-stained sections. *Foxd1, forkhead box D1*; *Phd*, *prolyl-4-hydroxylase domain*.

Figure S8. Normal renal development in *Foxd1-Hif1a*$^{-/-}$ and *Foxd1-Hif2a*$^{-/-}$ mutant mice. (**A**) Representative images of periodic acid-Schiff (PAS)–stained kidney sections (top), and cluster of differentiation (CD)31 and alpha actin-2 (ACTA2) immunohistochemistry (IHC) staining (middle and lower panels) for Cre^- control (*Foxd1*$^{+/+}$ *Hif1a*$^{fl/fl}$), *Foxd1-Hif1a*$^{-/-}$, or *Foxd1-Hif2a*$^{-/-}$ kidneys at postnatal day (P) 14. Asterisks indicate glomeruli, and arrows indicate renal tubules with PAS-positive brush borders. Bar = 100 μm. Although no differences in total body and kidney weights were observed between *Foxd1-Hif2a*$^{-/-}$mutants and controls, total body weight for *Foxd1-Hif1a*$^{-/-}$mutants was 4.6 ± 0.2 g and that for Cre^- littermate controls was 5.2 ± 0.06 g (n = 4 each; $P = 0.014$); kidney weight was 28.5 ± 0.7 mg for *Foxd1-Hif1a*$^{-/-}$ mutants and 32.9 ± 0.6 mg for Cre^- controls (n = 8 each; $P < 0.001$). (**B**) *Erythropoietin* (*Epo*) and mRNA levels of nephron segment and vascular markers in whole-kidney homogenates from *Foxd1-Hif1a*$^{-/-}$ or *Foxd-Hif2a*$^{-/-}$ compared with Cre^- littermate controls (n = 4 for *Foxd1-Hif1a*$^{-/-}$ and control; n = 3 for *Foxd1-Hif2a*$^{-/-}$ mice and control). Data are represented as mean ± SEM; 2-tailed Student's *t*-test; $^*P < 0.05$ and $^{**}P < 0.01$. *Aqp1*, *aquaporin 1*; *Aqp2*, *aquaporin 2*; *Foxd1*, *forkhead box D1;* HIF, hypoxia-inducible factor; *NaPi2a*, *sodium-phosphate cotransporter-2a*; *Ncc NaCl cotransporter*; *Nkcc2*, *Na-K-2Cl cotransporter*; *Phd*, *prolyl-4-hydroxylase domain*; *Scnn1a*, *sodium channel epithelial 1 alpha subunit*;*Trpv5*, *transient receptor potential cation channel subfamily V member 5*.

Supplementary Materials and Methods.

Supplementary material is linked to the online version of the paper at www.kidney-international.org.

REFERENCES

1. Dunwoodie SL. The role of hypoxia in development of the mammalian embryo. *Dev Cell*. 2009;17:755–773.
2. Semenza GL. Oxygen sensing, hypoxia-inducible factors, and disease pathophysiology. *Annu Rev Pathol*. 2014;9:47–71.
3. Kaelin WG Jr, Ratcliffe PJ. Oxygen sensing by metazoans: the central role of the HIF hydroxylase pathway. *Mol Cell*. 2008;30:393–402.
4. Marsal K. Intrauterine growth restriction. *Curr Opin Obstet Gynecol*. 2002;14:127–135.
5. Rueda-Clausen CF, Morton JS, Davidge ST. Effects of hypoxia-induced intrauterine growth restriction on cardiopulmonary structure and function during adulthood. *Cardiovasc Res*. 2009;81:713–722.
6. Moore LG, Charles SM, Julian CG. Humans at high altitude: hypoxia and fetal growth. *Respir Physiol Neurobiol*. 2011;178:181–190.
7. Wilkinson LJ, Neal CS, Singh RR, et al. Renal developmental defects resulting from in utero hypoxia are associated with suppression of ureteric beta-catenin signaling. *Kidney Int*. 2015;87:975–983.
8. Keller G, Zimmer G, Mall G, et al. Nephron number in patients with primary hypertension. *N Engl J Med*. 2003;348:101–108.
9. Hoy WE, Hughson MD, Bertram JF, et al. Nephron number, hypertension, renal disease, and renal failure. *J Am Soc Nephrol*. 2005;16:2557–2564.
10. Little MH, McMahon AP. Mammalian kidney development: principles, progress, and projections. *Cold Spring Harb Perspect Biol*. 2012;4. pii: a008300.
11. Krause M, Rak-Raszewska A, Pietila I, et al. Signaling during kidney development. *Cells*. 2015;4:112–132.

12. Hatini V, Huh SO, Herzlinger D, et al. Essential role of stromal mesenchyme in kidney morphogenesis revealed by targeted disruption of winged helix transcription factor BF-2. *Genes Dev*. 1996;10:1467–1478.
13. Levinson RS, Batourina E, Choi C, et al. Foxd1-dependent signals control cellularity in the renal capsule, a structure required for normal renal development. *Development*. 2005;132:529–539.
14. Das A, Tanigawa S, Karner CM, et al. Stromal-epithelial crosstalk regulates kidney progenitor cell differentiation. *Nat Cell Biol*. 2013;15:1035–1044.
15. Gomez IG, Duffield JS. The FOXD1 lineage of kidney perivascular cells and myofibroblasts: functions and responses to injury. *Kidney Int Suppl (2011)*. 2014;4:26–33.
16. Fetting JL, Guay JA, Karolak MJ, et al. FOXD1 promotes nephron progenitor differentiation by repressing decorin in the embryonic kidney. *Development*. 2014;141:17–27.
17. Nakagawa N, Xin C, Roach AM, et al. Dicer1 activity in the stromal compartment regulates nephron differentiation and vascular patterning during mammalian kidney organogenesis. *Kidney Int*. 2015;87:1125–1140.
18. Freeburg PB, Robert B, St John PL, Abrahamson DR. Podocyte expression of hypoxia-inducible factor (HIF)-1 and HIF-2 during glomerular development. *J Am Soc Nephrol*. 2003;14:927–938.
19. Bernhardt WM, Schmitt R, Rosenberger C, et al. Expression of hypoxia-inducible transcription factors in developing human and rat kidneys. *Kidney Int*. 2006;69:114–122.
20. Steenhard BM, Freeburg PB, Isom K, et al. Kidney development and gene expression in the HIF2alpha knockout mouse. *Dev Dyn*. 2007;236:1115–1125.
21. Haase VH. HIF-prolyl hydroxylases as therapeutic targets in erythropoiesis and iron metabolism. *Hemodial Int*. 2017;21(suppl 1):S110–S124.
22. Humphreys BD, Lin SL, Kobayashi A, et al. Fate tracing reveals the pericyte and not epithelial origin of myofibroblasts in kidney fibrosis. *Am J Pathol*. 2010;176:85–97.
23. Kobayashi A, Mugford JW, Krautzberger AM, et al. Identification of a multipotent self-renewing stromal progenitor population during mammalian kidney organogenesis. *Stem Cell Reports*. 2014;3:650–662.
24. Bertout JA, Patel SA, Simon MC. The impact of O2 availability on human cancer. *Nat Rev Cancer*. 2008;8:967–975.
25. Carmeliet P, Jain RK. Molecular mechanisms and clinical applications of angiogenesis. *Nature*. 2011;473:298–307.
26. Kobayashi H, Liu Q, Binns TC, et al. Distinct subpopulations of FOXD1 stroma-derived cells regulate renal erythropoietin. *J Clin Invest*. 2016;126:1926–1938.
27. Hartman HA, Lai HL, Patterson LT. Cessation of renal morphogenesis in mice. *Dev Biol*. 2007;310:379–387.
28. Rumballe BA, Georgas KM, Combes AN, et al. Nephron formation adopts a novel spatial topology at cessation of nephrogenesis. *Dev Biol*. 2011;360:110–122.
29. Kapitsinou PP, Liu Q, Unger TL, et al. Hepatic HIF-2 regulates erythropoietic responses to hypoxia in renal anemia. *Blood*. 2010;116:3039–3048.
30. Figueroa H, Lozano M, Suazo C, et al. Intrauterine growth restriction modifies the normal gene expression in kidney from rabbit fetuses. *Early Hum Dev*. 2012;88:899–904.
31. Tang J, Zhu Z, Xia S, et al. Chronic hypoxia in pregnancy affected vascular tone of renal interlobar arteries in the offspring. *Sci Rep*. 2015;5:9723.
32. Gonzalez-Rodriguez P Jr, Tong W, Xue Q, et al. Fetal hypoxia results in programming of aberrant angiotensin ii receptor expression patterns and kidney development. *Int J Med Sci*. 2013;10:532–538.
33. Schley G, Scholz H, Kraus A, et al. Hypoxia inhibits nephrogenesis through paracrine Vegfa despite the ability to enhance tubulogenesis. *Kidney Int*. 2015;88:1283–1292.
34. Iyer NV, Kotch LE, Agani F, et al. Cellular and developmental control of O2 homeostasis by hypoxia-inducible factor 1 alpha. *Genes Dev*. 1998;12:149–162.
35. Ryan HE, Lo J, Johnson RS. HIF-1 alpha is required for solid tumor formation and embryonic vascularization. *EMBO J*. 1998;17:3005–3015.
36. Wang SS, Gu YF, Wolff N, et al. Bap1 is essential for kidney function and cooperates with Vhl in renal tumorigenesis. *Proc Natl Acad Sci U S A*. 2014;111:16538–16543.
37. Kapitsinou PP, Sano H, Michael M, et al. Endothelial HIF-2 mediates protection and recovery from ischemic kidney injury. *J Clin Invest*. 2014;124:2396–2409.
38. Koury MJ, Haase VH. Anaemia in kidney disease: harnessing hypoxia responses for therapy. *Nat Rev Nephrol*. 2015;11:394–410.
39. Appelhoff RJ, Tian YM, Raval RR, et al. Differential function of the prolyl hydroxylases PHD1, PHD2, and PHD3 in the regulation of hypoxia-inducible factor. *J Biol Chem*. 2004;279:38458–38465.
40. Berra E, Benizri E, Ginouves A, et al. HIF prolyl-hydroxylase 2 is the key oxygen sensor setting low steady-state levels of HIF-1alpha in normoxia. *EMBO J*. 2003;22:4082–4090.
41. Minamishima YA, Moslehi J, Padera RF, et al. A feedback loop involving the Phd3 prolyl hydroxylase tunes the mammalian hypoxic response in vivo. *Mol Cell Biol*. 2009;29:5729–5741.
42. Takeda K, Ho VC, Takeda H, et al. Placental but not heart defects are associated with elevated hypoxia-inducible factor alpha levels in mice lacking prolyl hydroxylase domain protein 2. *Mol Cell Biol*. 2006;26:8336–8346.
43. Gruber M, Hu CJ, Johnson RS, et al. Acute postnatal ablation of Hif-2alpha results in anemia. *Proc Natl Acad Sci U S A*. 2007;104:2301–2306.
44. Ryan HE, Poloni M, McNulty W, et al. Hypoxia-inducible factor-1alpha is a positive factor in solid tumor growth. *Cancer Res*. 2000;60:4010–4015.